Available online at www.sciencedirect.com
ScienceDirect
International Journal of Pressure Vessels and Piping 84 (2007) 708–715
INTERNATIONAL JOURNAL OF Pressure Vessels and Piping
www.elsevier.com/locate/ijpvp

Effect of plastic prestrain on the crack tip constraint of pipeline steels

P.A. Eikrem[a], Z.L. Zhang[a,*], B. Nyhus[b]

[a]Department of Structural Engineering, Norwegian University of Science and Technology (NTNU), Trondheim, Norway
[b]SINTEF Materials and Chemistry, Trondheim, Norway

Received 19 February 2007; received in revised form 17 July 2007; accepted 1 August 2007

Abstract

Before and during operation, pipelines may suffer from plastic pre-deformation due to accidental loading, cold bending and ground movement. Plastic prestrain not only modifies steel's yield and flow properties but also influences its fracture performance. This paper focuses on the effect of prestrain history on crack driving force and crack tip constraint. A single-edge notched tension specimen has been selected for the study and the crack is assumed to exist before a prestrain history was applied. The results show that prestrain history has a strong effect on the crack tip stress field. A new parameter has been proposed to characterize the prestrain-induced crack tip constraint. For the same crack tip opening displacement level, prestrain history will elevate the crack tip stress field. The prestrain-induced constraint decreases with the increase of loading.

Keywords: Prestrain; Prestrain effect; Crack tip constraint; Crack tip stress field

1. Introduction

Steel pipelines are often subject to plastic deformation due to accidental loading, cold bending and ground movement, and the effect of the plastic deformation (prestrain history) on further deformation capability and functionality should be assessed. Pipe reeling (Fig. 1) is a typical example where the effect of plastic prestrain history on deformation and fracture behaviour needs to be quantified. In order to properly tackle the problem, the prestrain history and resulting plastic anisotropy should be precisely predicted first, using constitutive models capable of describing cyclic and non-linear material behaviour [1]. The next step is to study the effect of prestrain history on further deformation and fracture behaviour. It is known that prestrain history can influence in a detrimental manner the local failure mechanisms and macroscopic fracture initiation toughness and fatigue properties [2–7]. Most of the studies carried out in the literature focus on the effect of homogeneous prestrain effect on fracture toughness. The test specimens were first subject to a homogeneous prestrain history and a crack was introduced afterwards. In real pipe-laying operation, cracks due to welding defects may exist before a reeling process is started and it is interesting to study how reeling-induced prestrain history affects the crack driving force and crack tip stress field. The effect on crack tip stress field is important because of its strong influence on fracture toughness. The effect of prestrain history is a complex issue and this paper limits the scope to one symmetric prestrain cycle. A single-edge notched tension (SENT) specimen has been chosen for the study. It has been demonstrated both theoretically and experimentally that the SENT specimen is a good representation of the pipe sections in terms of fracture toughness measurements [8].

In the following, the concept of crack tip constraint and its latest development are briefly reviewed first. Crack tip constraint is a recent concept in fracture mechanics, which can explain the apparent dependence of fracture toughness on specimen geometry, crack size, loading, yield strength mismatch as well as residual stress. Numerical procedure, including the specimen geometry, materials and finite element models are described in Section 3. The results are discussed in Section 4. Based on the results, a three-parameter formulation (CTOD-Q-P) is presented in

*Corresponding author. Tel.: +47 73592530.
E-mail address: zhiliang.zhang@ntnu.no (Z.L. Zhang).

0308-0161/$ - see front matter
doi:10.1016/j.ijpvp.2007.08.007

Section 5 to characterize the crack tip stress field in the presence of prestrain history. The paper is closed with summary and conclusions.

2. Crack tip constraints

The fundamental concept in the conventional elastic–plastic fracture mechanics is that the crack tip stress field can be described by a single parameter, the J-integral (HRR field) or crack tip opening displacement (CTOD), and material fracture toughness obtained from one specimen can be transferred to other specimens. There are, however, many scenarios where the conventional single-parameter approach becomes invalidated and crack tip stress fields are influenced by the level of crack tip constraint. In the following, the constraints due to geometry, material mismatch, residual stress and plastic strain history are briefly reviewed.

2.1. Geometrical constraint—J–Q formulation

It is now well understood that the single-parameter-based approach has a limited range of validity. For homogeneous materials, the crack tip stress field is not uniquely controlled by J or CTOD. The crack tip stress field is also influenced by specimen dimensions, crack length to specimen width ratio as well as loading mode. A second parameter based on the elastic T stress has been proposed by Betegon and Hancock [9] to describe the crack tip stress field. For elastic–plastic problems, O'Dowd and Shih [10,11] proposed a J–Q formulation to characterize the effect of geometry constraint on the crack tip stress field, where J sets the deformation level and Q is a stress triaxiality parameter which is a direct measure of the stress field that is related to a reference field usually described by the HRR field. Under small-scale yield conditions it has been shown that the Q parameter can be uniquely linked to the elastic T stress [10]. However, in finite geometries under large-scale yielding, the one-to-one relation is lost. The J–Q theory can be written as

$$\sigma_{ij}(r,\theta) = \sigma_{ij}^{0}(r,\theta,J,\sigma_0,n) + \sigma_{ij}^{\mathrm{Diff}}(\sigma_0,Q), \tag{1}$$

where r and θ are polar coordinates with origin at the crack tip, σ_0 and n are the yield stress and plastic strain-hardening exponent, σ_{ij}^{0} is the reference stress field controlled by the J and $\sigma_{ij}^{\mathrm{Diff}}$ is the difference field. It has been shown by O'Dowd and Shih that the difference field for a wide range of constraint levels is relatively independent of both the normalized distance and angular position in the forward sector of the crack tip region [10,11]. The shear component of the difference field is approximately zero. The difference stress field can therefore be approximated by a hydrostatic stress field with Q as the normalized amplitude:

$$\sigma_{ij}^{\mathrm{Diff}}(\sigma_0,Q) \approx \sigma_0 Q \delta_{ij}, \tag{2}$$

where δ_{ij} is the Kronecker delta. It must be noted that the J–Q description deviates gradually from the numerical crack tip stress fields from moderate-scale yielding to large-scale yielding, in particular for bending dominated specimens. Q could become strongly distance-dependent for bending specimen at a high load level [12].

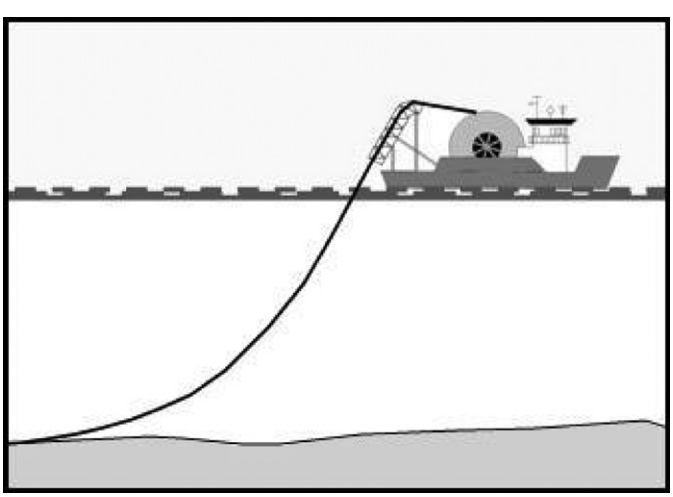

Fig. 1. Schematic plot of the pipe reeling process.

2.2. Material mismatch-induced constraint—J–Q–M formulation

For interface cracks in an inhomogeneous material system such as a weldment, there are two types of constraints at the crack tip. For the same J or CTOD, crack tip stress field will be influenced not only by the geometric constraint but also by the strength mismatch between different material properties [13,14]. Numerical studies by Zhang et al. [13] have found that the effect of material mismatch on the crack tip stress field can be described by a material mismatch constraint parameter M. It has also been found that the effect of geometry and material mismatch to a certain degree is independent of each other and can be separated. Based on this observation, a so-called J–Q–M formulation has been proposed to characterize the effect of both geometry and material mismatch constraints on the crack tip stress field. In the J–Q–M formulation, J defines the deformation level at the crack tip, while the actual stress state at the crack tip is governed by additional constraint parameters Q and M. The J–Q–M formulation is written as

$$\sigma_{ij}(r,\theta) = \sigma_{ij}^{0}(r,\theta,J,\sigma_0,n) + Q\sigma_0\delta_{ij} + M_0\sigma_0 f_{ij}(\theta+12\beta,n), \tag{3}$$

where σ_0 and n are the yield stress and hardening exponent of the reference material, f_{ij} represents the angular function of the mismatch-induced difference field, $\beta = 0$ for overmatch and $\beta = 1$ for undermatch [13]. Eq. (3) is valid for both the reference and mismatch materials, and is most accurate for the reference material. Weldment fracture problems with crack in the centre of weld metal has been

studied by Burstow et al. [15] and Betegon and Penuelas [16] and similar formulations of the stress field have been discussed.

2.3. Residual stress-induced constraint CTOD–Q–R formulation

In welded components, cracked specimens may suffer from residual stresses and the residual stresses will influence the crack tip stress field. Recently, the effect of residual stress on the crack tip stress field has been studied by Liu et al. [17]. In the case of residual stress-induced constraint, CTOD has been preferred as a crack driving force because the J-integral becomes questionable in the presence of residual stress. Their results show that a three-parameter approach (CTOD, Q and R) can be used to characterize the crack tip stress field in the presence of residual stress, where CTOD sets the size scale over which large stresses and large strains develop, and Q and R characterize the constraint level. R can be interpreted as a parameter governing a hydrostatic stress ahead of the crack tip. Both Q and R can be interpreted as hydrostatic stress field parameters; however, they possess different features [17]. Q negatively increases with the plastic deformation while R usually starts with a positive value and decreases to zero when the plastic deformation is large enough. The new formulation can be written as

$$\sigma_{ij}(r,\theta) = \sigma_{ij}^{0}(r,\theta,\delta,\sigma_0,n) + Q\sigma_0\delta_{ij} + R\sigma_0\delta_{ij}, \tag{4}$$

where δ denotes the CTOD. An extensive study on the effect of crack driving force and crack tip stress field is being performed at the ongoing project—Residual Stress Simulation and Integrity Assessment at NTNU and SINTEF.

2.4. Prestrain history-induced constraint

Ernst has recently studied the effect of prestrain history on the fracture mechanics parameters [7]. A SENT specimen has been applied for the study of material resistance curve evolution with prestrain history. Tow types of resistance curves—history-independent resistance and material memory resistance—have been discussed without exploring the effect of prestrain history on the crack tip stress field. In a preliminary study [18], the complete Gurson model developed by the authors [19] has been used to study the effect of crack resistance curves. It has been found that prestrain history significantly alters the crack tip stress field. No systematic study was performed. This study is a continuation of [18]. In this study, focus will be placed on the characterization of the prestrain-induced crack tip constraint.

3. Numerical procedures

Pipe geometry represents a special category of low constraint components. In the past years, efforts have been spent to search for appropriate fracture mechanics specimens, which possess similar crack tip constraint levels as the cracks found in a pipe. Both experimental studies and numerical analyses have demonstrated that the crack tip constraint in a SENT is a good representation of the pipe. The SENT specimen has been chosen to study the effect of prestrain history in this paper. Fig. 2 schematically shows the SENT specimen geometry and finite element mesh used. A 2D plane strain model with four-node elements has been used. The initial crack size (a) considered is 4 mm and other dimensions are $a/w = 0.143$ and $L/w = 4.1$. The specimen dimensions and applied loading have been chosen such that buckling during compression is avoided. A remote homogeneous displacement-controlled boundary condition (clamped) was applied. Because of the symmetry, half of the SENT specimen has been modelled in finite element analysis. During the prestrain cycle the crack faces will be partly closed. A rigid analytical plane has been defined in the model to simulate the contact of crack faces. The rigid plane is shown in Fig. 2b as a horizontal line. ABAQUS with Mises plasticity and non-linear geometry option (NLGEOM) was used for the analyses.

A model material with following power law hardening model has been used:

$$\sigma_f = \sigma_0\left(1 + \frac{\bar{\varepsilon}^p}{\varepsilon_0}\right)^n, \tag{5}$$

where n is the strain-hardening exponent, σ_0 and ε_0 are the yield stress and yield strain, and σ_f and $\bar{\varepsilon}^p$ are the flow stress and equivalent plastic strain, respectively. The same material model has been used previously to investigate the material mismatch-induced crack tip constraint [13]. The material considered here has a yield stress 460 MPa and plastic strain-hardening exponent 0.05. The material data used are representative of the X65 pipe steels. The Young's modulus is 207 GPa and Poisson ratio is 0.3. It

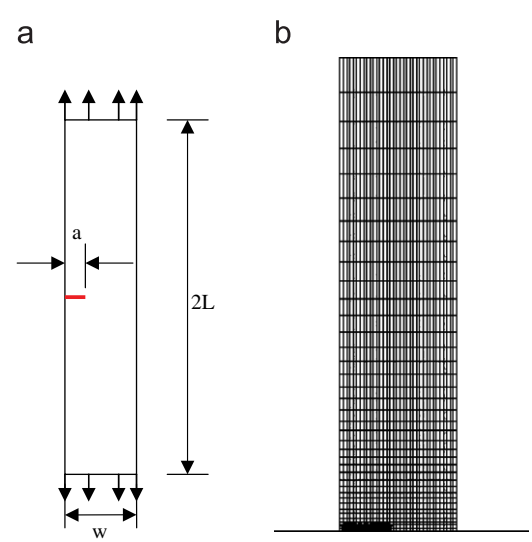

Fig. 2. (a) Schematic plot of the SENT specimen and (b) the finite element model used in the analysis.

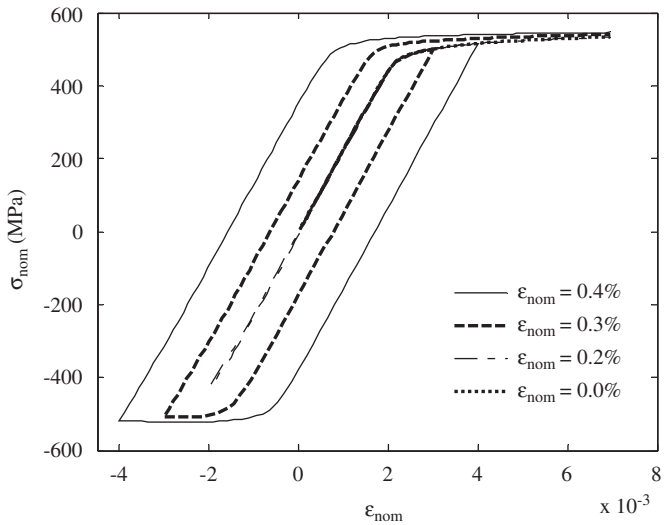

Fig. 3. Nominal stress versus nominal strain curves.

should be noted that the material is initially isotropic and an isotropic hardening model in ABAQUS has been assumed in this study.

Industrial reeling process contains multi-prestrain cycles [7]. In this study, a simpler problem was studied. Only single symmetric prestrain cycles were considered. Prestrain was characterized by the averaged remote strain (nominal strain), which is measured by dividing the applied displacement by the initial half-specimen length L. The symmetrical prestrain history was applied first in tension and then in compression. The nominal strain amplitudes varied from 0% to 0.4%. After the symmetric prestrain process the specimen was loaded further (re-loading) to a nominal strain about 0.7%. The amplitudes of the prestrains in this study are close to the prestrain levels considered in [7]. Fig. 3 shows the cyclic nominal stress–strain curves for the cases analysed. Material's yield strain is 0.22% and it can be observed from Fig. 3 that there is no significant difference in nominal stress strain curves between the case with prestrain 0.2% and the monotonic loading case. In Section 4, the results of crack driving force as well as the crack tip stress field are presented.

4. Results

Because the J-integral is originally developed for non-linear elastic material and is not well suited for cyclic plasticity problem, the CTOD has been used as the crack driving force parameter. It is known that for monotonic loading and non-linear elastic material, an intrinsic relation between the CTOD and J-integral exists [20]. However, this relation is not clear in the prestrain problem considered. The CTOD was selected as a result of convenience, and it is beyond the scope of this paper to discuss which parameter is the most appropriate one.

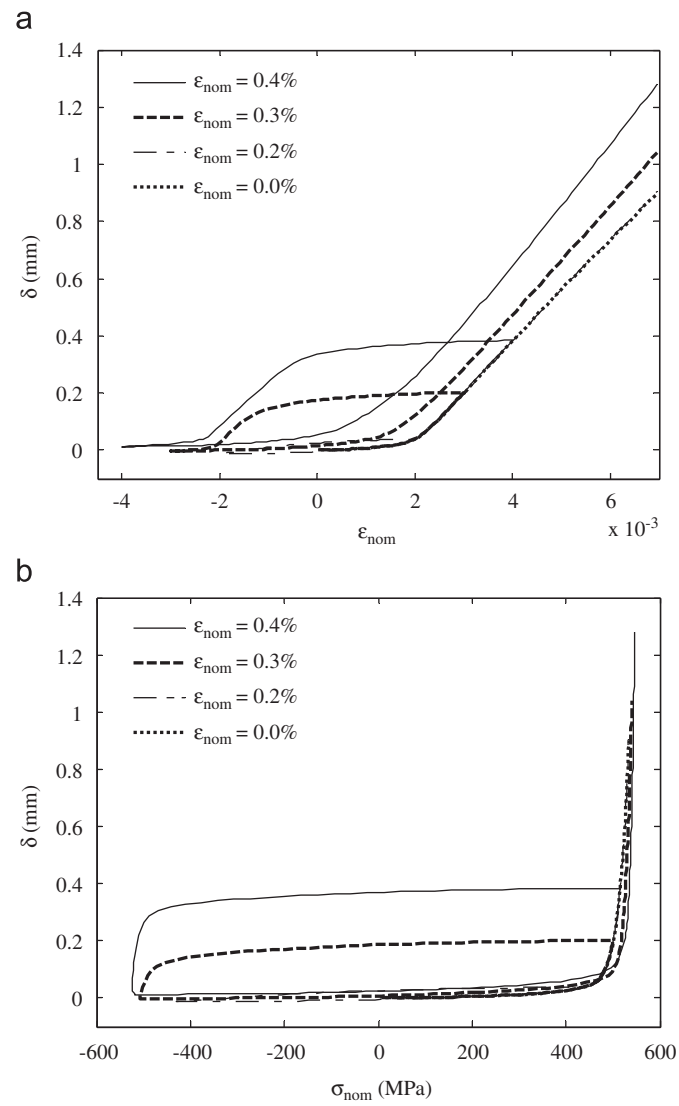

Fig. 4. (a) CTOD versus remote strain and (b) CTOD versus nominal stress.

4.1. CTOD–remote strain curves

For monotonic loading, the CTOD versus nominal strain curve of a SENT specimen can be divided into a global elastic region and a global plastic region. The global elastic region can be characterized by a linear curve and a quadratic transition region, and a linear curve with steeper gradient is usually the characteristic of the global plastic region [21,22]. The crack tip opening displacement versus nominal strain curves for the cases analysed are shown in Fig. 4a. In all the analyses the prestrain cycle begins with a tension first. As a usual practice, the crack is modelled with an initial opening. The initial opening considered in this study is 0.02 mm and, therefore, a maximum closure 0.02 mm is possible. In the loading path, a typical CTOD versus strain curve can be observed. The CTOD increases slowly in the global elastic region and rapidly when substantial yielding has reached. Similar behaviour can be observed in the reverse loading stage. In the loading,

reverse loading and re-loading process an elastic–plastic CTOD–strain loop is created. The size of the loop increases with the increase of prestrain level. It can be seen that the loop is very small for the case with prestrain 0.2%. During the re-loading process, the length of the global elastic region becomes prolonged and the global plastic region starts at smaller nominal strain, compared with the monotonic loading case. A smoother transition region between the global elastic and global plastic region can also be seen for the case with prestrain history. This behaviour can be explained by the strong local hardening at the crack tip. The CTOD curves also become diverged in the re-loading process. It should be noted that no ductile crack growth has been considered in the present analyses and the resulting CTOD value is therefore smaller than those reported in [7].

The CTOD versus nominal stress curves for the cases analysed are shown in Fig. 4b. A CTOD–stress-like loop behaviour can also be seen. However, the re-loading CTOD–stress curves are converging rather than diverging as the CTOD–strain curves. This observation can be linked to the results in Fig. 3. For elastic–plastic materials, stress is less sensitive than the strain. This is the reason why the strain-based design is being utilized in pipeline technology [23].

In real industrial applications, cracked components are often unloaded after a prestrain history before reloading. It is interesting to observe how the crack driving force develops from the load-free condition. The CTOD–strain curves in Fig. 4a have been re-plotted from their load-free conditions in Fig. 5. The increment with zero nominal stress in Fig. 3 from the second cycle for each case was identified as the load-free condition. Fig. 5 indicates that the effect of prestrain history on the crack driving force is negligible for the examined prestrain cycles and the material considered. It can be seen that the actual CTOD at zero nominal stress is not zero; the residual CTOD increases with the applied prestrain level. It should be noted that the CTOD versus strain from load-free condition in general depends on the applied prestrain level.

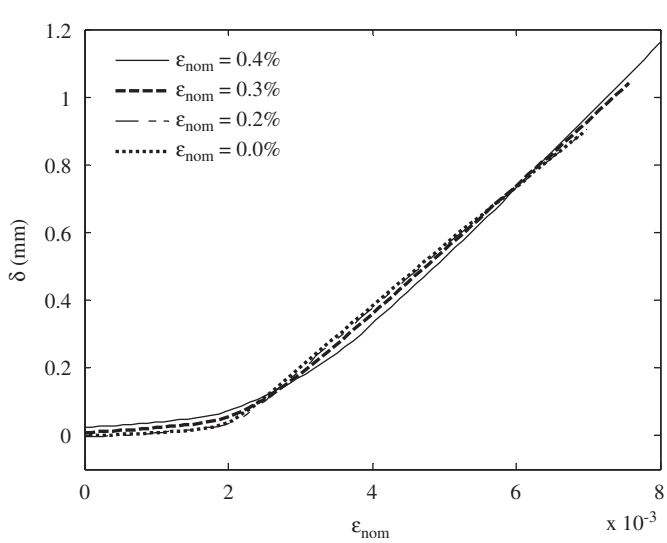

Fig. 5. CTOD versus strain from load-free conditions.

4.2. Crack tip stress distributions and constraints

In this study, only the distribution of the crack tip opening stress ($\sigma_{\theta\theta}$ at $\theta = 0$) has been studied. Fig. 6a shows the opening stress distribution as a function of CTOD in a monotonic loading case. The distance from the crack tip up to 10 times of the CTOD has been plotted. This range is believed to be of interest for both cleavage and ductile fracture. It can be clearly seen that the normalized stress distribution is not constant and it is now known that the reduction of the stress is due to the geometric constraint, Fig. 6b. The constraint parameter Q can be calculated from Fig. 6b. The Q stress was originally defined as

$$Q = \frac{\sigma_{\theta\theta} - \sigma_{\theta\theta}^{\mathrm{Ref}}}{\sigma_0}, \quad \text{at} \quad x/(J/\sigma_0) = 2, \quad \theta = 0, \tag{6}$$

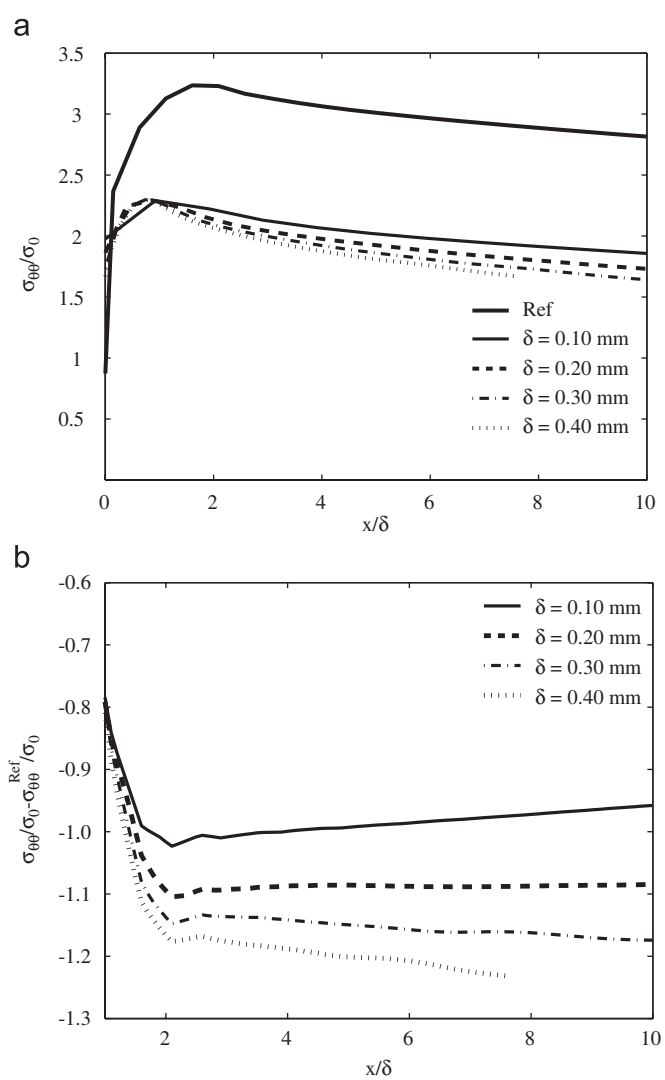

Fig. 6. (a) Opening stress distributions and (b) normalized difference fields. Monotonic loading and no prestrain history was applied.

where x is the distance from the crack tip along the x-axis ($\theta = 0$).

Because of the use of CTOD as crack driving force, the following definition of Q has been used:

$$Q = \frac{\sigma_{\theta\theta} - \sigma_{\theta\theta}^{\mathrm{Ref}}}{\sigma_0}, \quad \text{at} \quad x/\delta = 4, \quad \theta = 0. \tag{7}$$

It can be seen from Fig. 6 that $\sigma_{\theta\theta} - \sigma_{\theta\theta}^{\mathrm{Ref}}$ calculated for the monotonic loading case will only change in a small degree in the range of $2 < x/\delta < 10$ for the SENT specimen. The gradient of the opening stress distribution becomes steeper when the CTOD increases. The reference solution $\sigma_{\theta\theta}^{\mathrm{Ref}}$ can be obtained from the well-known HRR solution or from a finite element solution of a boundary layer model under small-scale yielding conditions. In the present study, the boundary layer model applied in [13] was used.

The prestrain history will influence the stress distribution. Fig. 7 compares the opening stress distributions with different prestrain histories. Three prestrain histories of 0.2%, 0.3% and 0.4% have been considered. At a CTOD 0.1 mm, a maximum opening stress about 2.3 times the yield stress can be observed for the case with monotonic loading. However, the maximum opening stress for the case with prestrain 0.4% approaches about 2.6 times the yield stress. What is interesting to observe is that the elevation of the opening stress due to prestrain history applies to the whole range of interest, $x \leqslant 10\delta$. Fig. 7b shows that when the CTOD increases, the elevation of the opening stress due to the prestrain history becomes less significant. It is known from Fig. 6 that the stress distribution becomes steeper at higher CTOD. It seems that this behaviour is the same for the cases with prestrain history.

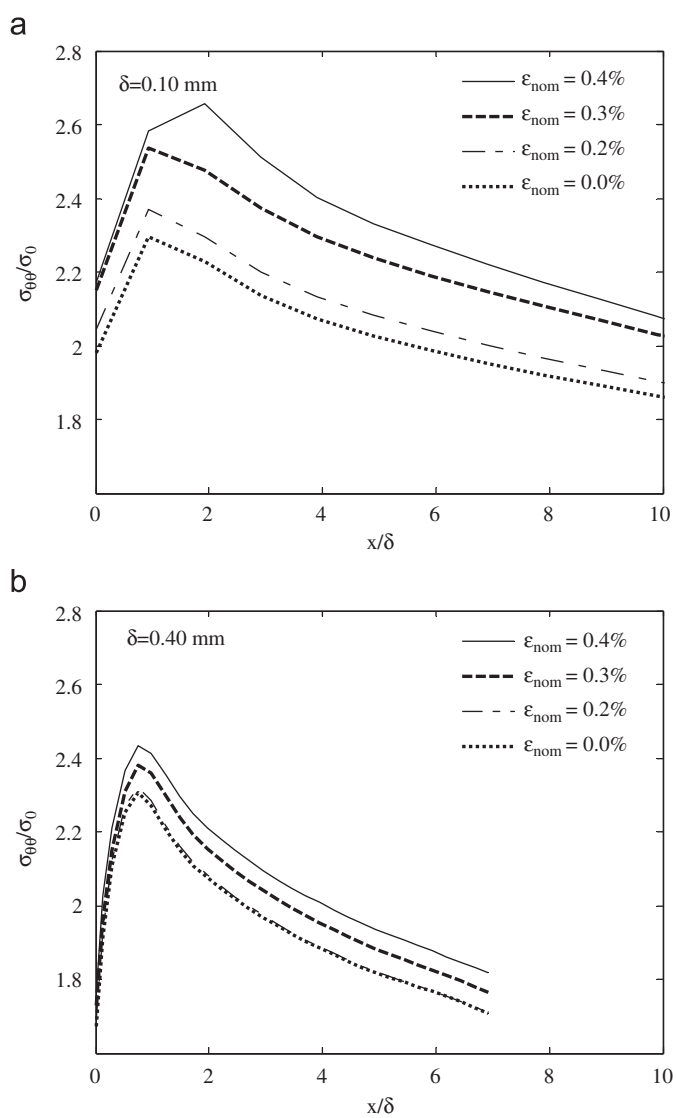

Fig. 7. Opening stress distributions with different prestrain history at (a) CTOD 0.1 mm and (b) 0.4 mm.

5. Approximate structure of the crack tip stress fields

5.1. CTOD–Q–P three-parameter formulation

In order to quantify the effect of prestrain effect on the crack tip stress field, the stress field due to the prestrain history has been separated from the total stress distribution in Fig. 7. The stress due to the prestrain effect is called the difference field. It is calculated as

$$\frac{\Delta\sigma_{\theta\theta}}{\sigma_0} = \left(\frac{\sigma_{\theta\theta}}{\sigma_0}\right)_{\varepsilon} - \left(\frac{\sigma_{\theta\theta}}{\sigma_0}\right)_{\varepsilon=0}, \tag{8}$$

where $(\sigma_{\theta\theta}/\sigma_0)_{\varepsilon}$ implies the case with prestrain history and $(\sigma_{\theta\theta}/\sigma_0)_{\varepsilon=0}$ denotes the monotonic loading case. The difference fields at different CTOD for the case with prestrain 0.4% and 0.2%, respectively, are plotted in Fig. 8. It is interesting to observe from Fig. 8 that except the cases with small CTOD, the difference stress field due to prestrain effect seems to be rather independent of the normalized distance from the crack tip. In order to quantify the prestrain effect on the crack tip stress field, the following new constraint parameter has been proposed:

$$P = \left(\frac{\Delta\sigma_{\theta\theta}}{\sigma_0}\right)_{x/\delta=4} = \left\{\left(\frac{\sigma_{\theta\theta}}{\sigma_0}\right)_{\varepsilon} - \left(\frac{\sigma_{\theta\theta}}{\sigma_0}\right)_{\varepsilon=0}\right\}_{x/\delta=4}, \quad \theta = 0. \tag{9}$$

The new constraint parameter P versus CTOD is plotted in Fig. 9. It is interesting to note that even for the case with 0.2% prestrain, where no significant effect on the nominal stress–strain curve can be noticed, the opening stress increased more than 10% of yield stress at CTOD 0.05 mm compared with the monotonic loading case. The prestrain-induced constraint P decreases with the increase of CTOD. When the CTOD is 0.4 mm the effect of prestrain effect on the crack tip stress field can be neglected for the case with prestrain 0.2%.

Based on the above observations, the following approximate formulation can be used to describe the crack tip stress field with a prestrain history:

$$\sigma_{\theta\theta}^{\varepsilon}(x) = \sigma_{\theta\theta}^{\varepsilon=0}(x, \delta, \sigma_0, n) + Q + P \quad \text{at} \quad \theta = 0. \tag{10}$$

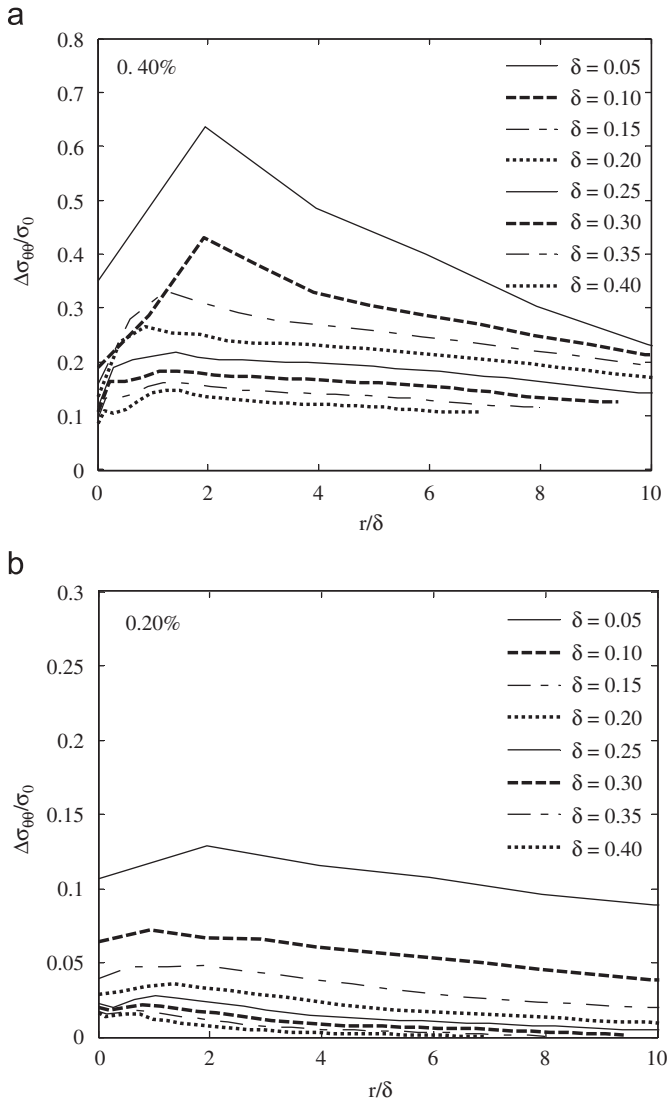

Fig. 8. The difference stress fields as a function of CTOD (a) for the case with prestrain 0.4% and (b) for the case with prestrain 0.2%.

Eq. (10) uses three global parameters (CTOD, Q and P) to approximate the crack tip stress field. The three-parameter formulation can be further applied to quantify the prestrain-induced constraint effect on fracture toughness, for example, using the RKR criterion [24], in a similar way as the application of the J–Q–M theory [13,14,25]. A detailed procedure and practical examples of the application of the J–Q–M theory are given in [25].

5.2. Nature and origin of the prestrain-induced crack tip constraint

The finite element analysis results have shown that a plastic prestrain history applied to a SENT specimen after a crack is introduced will induce an additional crack tip constraint. Unlike the geometry-induced crack tip constraint Q that is usually negative and decreases with the plastic deformation, the prestrain-induced constraint P is normally positive and decreases to zero when the plastic deformation is sufficiently large. The prestrain-induced crack tip constraint P is primarily dependent on the applied prestrain level, nature of the prestrain cycles, specimen geometry and loading. A detailed study of the relation between P and these factors is out of the scope of the present study.

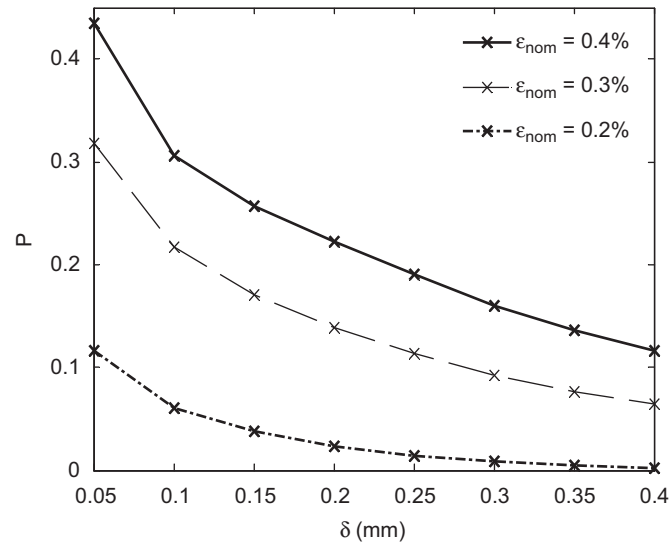

Fig. 9. Constraint parameter P as a function of CTOD.

The origin of P comes from the localized deformation at the crack tip during the prestrain cycle. Due to stress/strain concentration, a localized material zone at the crack tip with elevated yield strength and reduced strain hardening will be developed when a prestrain cycle is finished. A self-balance residual stress field also exists at the load-free condition [26]. In the reloading process, the SENT specimen actually consists of materials with different plastic properties. At the crack tip, the crack is surrounded by a zone with higher yield strength and is relatively more "elastic" compared with the rest of the specimen and also the specimen without a prestrain history. At the same CTOD, the opening stress in front of the crack tip is therefore higher than that in the case without prestrain. That explains why P is positive. With the increase of plastic deformation, the effect of the "elastic" zone decreases and P approaches zero.

6. Concluding remarks

It is known that specimen geometry and loading mode, material strength mismatch and residual stress field all influence the crack tip constraint. In this paper, the effect of prestrain history on the crack tip stress field has been investigated for the first time. A SENT specimen exposed to a single symmetric prestrain cycle was used. The SENT specimen was chosen because it is probably the most appropriate specimen in terms of crack tip constraint to represent the surface cracks in a pipe [8]. The prestrain cycle started with tension first. The loading was reversed when a given prestrain is reached. The specimen was

reloaded up to a higher CTOD. The result shows that prestrain does not have significant influence on the correlation between crack driving force and global deformation for the examined strain history cases. However, it has been found that prestrain history will invalidate the one-to-one relation between the crack driving force and crack tip stress field. Prestrain history induces a crack tip constraint, which will elevate the crack tip stress.

In this study, the stress field induced by the prestrain has been separated from the total numerical stress field (element method analysis). This field is called difference field. It is interesting to observe that the difference field is rather independent of the normalized crack tip distance. A new parameter P has been introduced to characterize the prestrain-induced constraint. With the new parameter, a three-parameter formulation (CTOD, Q and P) can be used to describe the crack tip stress field of prestrained specimens. It has been shown that P starts with a positive value and decreases with the increase of loading. The prestrain-induced constraint and its effect should be further taken into consideration of the fracture assessment of pipeline steels.

It should be noted that this study is just a small step forward towards the understanding of the prestrain effect on fracture behaviour of pipeline steels. A symmetric prestrain cycle with an isotropic hardening model has been considered. Pipe reeling or other industrial and service processes may involve multi-prestrain (both symmetric and non-symmetric) cycles and the first cycle may not necessary be tension. The question raised by Ernst [7] as to whether the material displays a history-independent resistance curve or material-memory resistance curve is still open. Prestrain history may not only influence the crack tip stress field but may also influence the failure mechanisms and change the failure modes. It has also recently been noticed that prestrain history will also influence the microvoid coalescence behaviour [27]. Microvoid nucleation, growth and coalescence are the main mechanisms for ductile fracture. Many of these topics are under investigation and will be reported elsewhere.

References

[1] Martinez M, Brown G. Evolution of pipe properties during reel-lay process: experimental characterisation and finite element modeling. In: Proceedings of the 24th international conference on offshore mechanics and Arctic engineering (OMAE 2005), Halkidiki, Greece, June 12–17, 2005.

[2] Fukuda N, Hagiwara N, Masuda T. Effect of prestrain on tensile and fracture properties of line pipes. J Offshore Mech Artic Eng 2005; 127:263–8.

[3] Enami K. The effects of compressive and tensile prestrain on ductile fracture initiation in steels. Eng Fract Mech 2005;72:1089–105.

[4] Qiu H, Enoki M, Hiraoka K, Kishi T. Effect of prestrain on fracture toughness of ductile structural steels under static and dynamic loading. Eng Fract Mech 2005;72:1624–33.

[5] Chae D, Bandstra JP, Koss DA. The effect of prestrain and strain-path changes on ductile fracture: experimental and computational modeling. Mater Sci Eng A 2000;285:165–71.

[6] Cosham A. A model of prestrain effects on fracture toughness. J Offshore Mech Arctic Eng 2001;123:182–90.

[7] Ernst H, Bravo RE, Daguerre F, Izquierdo A. Strain history effects on fracture mechanics parameters-application to reeling. In: Proceedings of the 24th international conference on offshore mechanics and Arctic engineering (OMAE 2005), Halkidiki, Greece, June 12–17, 2005.

[8] Nyhus B, Polanco ML, Ørjasæther O. SENT specimens an alternative to SENB specimens for fracture mechanics testing of pipelines. In: Proceedings of the 22nd international conference on offshore mechanics and Arctic engineering (OMAE 2002), June 8–13, 2001, Cancun, Mexico; 2003. p. 259–66.

[9] Betegon C, Hancock JW. Two-parameter characterization of elastic–plastic crack-tip fields. J Appl Mech 1991;58:104–10.

[10] O'Dowd NP, Shih CF. Family of crack-tip fields characterized by a triaxiality parameter—I. Structure of fields. J Mech Phys Solids 1991; 39:989–1015.

[11] O'Dowd NP, Shih CF. Family of crack-tip fields characterized by a triaxility parameter—II. Fracture application. J Mech Phys Solids 1991;40:939–63.

[12] Zhu X-K, Leis N. Bending modified J–Q theory and crack tip constraint quantification. Int J Fract 2006;141:115–34.

[13] Zhang ZL, Hauge M, Thaulow C. Two-parameter characterization of the near-tip stress fields for a bi-material elastic–plastic interface crack. Int J Fract 1996;79:65–83.

[14] Zhang ZL, Hauge M, Thaulow C. The effect of T stress on the near tip stress field of an elastic–plastic interface crack. In: Karihaloo BL, Mai Y-W, Ripley MI, Ritchie RO, editors. Proceedings of the ninth international congress on fracture, vol. 5, Sydney, 1997. p. 2643–50.

[15] Burstow MC, Howard IC, Ainsworth RA. The influence of constraint on crack tip stress fields in strength mismatched welded joints. J Mech Phys Solids 1998;46:845–72.

[16] Betegon C, Penuelas I. A constrainted based parameter for quantifying the crack tip stress fields in welded joints. Eng Fract Mech 2006;73:1865–77.

[17] Liu J, Zhang ZL, Nyhus B. Study on residual stress induced crack tip constraint, submitted for publication.

[18] Zhang ZL, Østby E, Nyhus B, Ødegård J. Prestrain history effect on ductile fracture of pipeline steels. In: Proceedings of the international seminar on application of high strength line pipe and assessment of pipeline 2006, Xi'an, China, June 2006.

[19] Zhang ZL, Thaulow C, Ødegård J. A complete Gurson model for ductile fracture. Eng Fract Mech 2000;67:155–68.

[20] Shih CF. Relationship between the J-integral and the crack opening displacement for stationary and extending cracks. J Mech Phys Solids 1981;29:305–26.

[21] Andersen TL. Fracture mechanics. 2nd ed. Boca Raton, FL: CRC Press; 1995.

[22] Jayadevan KR, Østby E, Thaulow C. Fracture response of pipelines subjected to large plastic deformation under tension. Int J Press Vessels Piping 2004;81:771–83.

[23] Østby E. Fracture control-offshore pipelines: new strain-based fracture mechanics equations including the effects of biaxial loading, mismatch and misalignment. In: Proceedings of the 24th international conference on offshore mechanics and Arctic engineering (OMAE 2005), 2005. p. 649–58.

[24] Ritchie RO, Knott JF, Rice JR. On the relationship between critical tensile stress and fracture toughness in mild steel. J Mech Phys Solids 1973;21:395–410.

[25] Zhang ZL, Hauge M, Thaulow C. Effects of crack size and weld metal mismatch on the HAZ cleavage toughness of weld plates. Eng Fract Mech 1997;57:653–64.

[26] Zhang ZL, Østby E, Nyhus B, Ødegård J, Verley R. Reeling induced residual stresses and its effect on the fracture behaviour of pipes with through thickness cracks. In: Proceedings of the international pipeline technology conference,Ostend, Belgium, 9–13 May 2004, p. 887–96.

[27] Zhang ZL, Skallerud B. Effect of prestrain history on microvoid coalescence, submitted for publication.